JOURNAL OF THERMOPHYSICS AND HEAT TRANSFER
Vol. 18, No. 3, July–September 2004

Effects of Gravity on the Performance of Pulsating Heat Pipes

Junjie Gu*
Carleton University, Ottawa, Ontario K1S 5B6, Canada
Masahiro Kawaji†
University of Toronto, Toronto, Ontario M5S 3E5, Canada
and
Ryosuke Futamata‡
Japan Aerospace Exploration Agency, Tsukuba 305-8505, Japan

Pulsating heat pipes made of a thin aluminium plate (250 × 60 × 2.2 mm) with small internal channels and charged with a refrigerant (R-114) have been tested under normal to high gravity (1–2.5 g_0) and reduced gravity ($\sim \pm 0.02\ g_0$) levels to investigate the effect of gravity on their heat transport characteristics. Reduced gravity experiments were performed aboard Falcon 20 aircraft flying parabolic trajectories, yielding about 20 s of reduced gravity at $\sim \pm 0.02\ g_0$. Under normal and hypergravity conditions, both the orientation of the pulsating heat pipe and locations of the heated and cooled sections affected the heat transfer performance. For example, large temperature fluctuations were observed when the heat pipe was oriented vertically and heated at the top. Under reduced gravity, however, the heat pipes showed better operating and heat transport performance than that under normal and hypergravity. These experiments have, for the first time, confirmed that pulsating heat pipes are capable of operating satisfactorily under reduced gravity and, thus, that they should be suitable for deployment in space applications. A theoretical analysis revealed the possibility that this type of a heat pipe with larger channel diameters (up to 5 mm for R114 as a working fluid) could work under microgravity, though they may not work on the ground.

Nomenclature

A_x	=	acceleration in x direction, m/s^2
A_y	=	acceleration in y direction, m/s^2
A_z	=	acceleration in z direction, m/s^2
D	=	diameter, m
d	=	diameter, m
E	=	energy, J
g, g_0	=	gravitational acceleration, 9.81 m/s^2
j^*	=	dimensionless velocity
k	=	thermal conductivity, W/(K · m)
L	=	length, m
q	=	heat transfer rate, W
Re	=	Reynolds number
r	=	radius, m
Su	=	Suratman number
V	=	velocity, m/s
We	=	Weber number
α	=	contact angle of liquid on wall surface
ΔT	=	temperature difference, K
μ	=	dynamic viscosity, kg/m · s; micro, $\times 10^{-6}$
ρ	=	density, kg/m^3
σ	=	surface tension, N/m

Subscripts

i	=	inner
k	=	kinetic
l	=	liquid; lower part of heat pipe model 2
max	=	maximum
s	=	surface
u	=	upper part of heat pipe model 2
v	=	vapor
1	=	pulsating heat pipe model 1
2	=	pulsating heat pipe model 2

Received 11 June 2003; revision received 28 January 2004; accepted for publication 6 March 2004.

*Assistant Professor, Department of Mechanical and Aerospace Engineering; jgu@mae.carleton.ca.
†Professor, Department of Chemical Engineering and Applied Chemistry; kawaji@ecf.utoronto.ca.
‡Researcher, Tsukuba Space Center.

Introduction

DEVELOPED in the 1990s (Ref. 1), pulsating heat pipes (PHPs), also referred to as open- or closed-loop oscillating heat pipes in the literature, possess outstanding heat transport performance and are increasingly used in the area of electronics cooling. For optimized design and a wider range of applications, such as advanced thermal control of aerospace hardware, however, it is necessary to better understand the working mechanism of PHPs under different conditions, including microgravity.

A PHP can be made from a long capillary tube bent into many turns, or a small continuous flow channel fabricated inside a metal plate, as shown schematically in Fig. 1, and partially filled with a working fluid such as a refrigerant. The evaporator and condenser sections are typically located at the opposite ends, and the working fluid undergoes phase change. The resulting two-phase (liquid/vapor) mixture travels back and forth between the evaporator and condenser sections. The inner diameter of the flow channel must be sufficiently small (0.5–2.0 mm), so that the vapor phase can form vapor plugs in the channel, resulting in a slug flow pattern. As heat is added to the evaporator section of the PHP, liquid is vaporized, causing the vapor volume to expand rapidly and causing pressure to increase, pushing the fluid away from the heated section. Simultaneously, vapor at the other end (condenser section) is condensed into liquid, causing a contraction in volume and reduction in pressure. As a result, a pulsating motion (as well as circulation) of the liquid slugs and vapor plugs occurs throughout the continuous channel in the entire heat pipe. Compared with the traditional heat pipes, the unique feature of PHPs is that there is no wick structure to return the condensate to the evaporator section, and, therefore, there is no countercurrent flow between the liquid and vapor. The fluid transport in PHPs is also much faster than that in the wicked

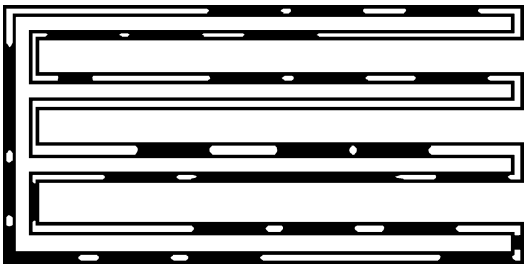

Fig. 1 Looped PHP.

heat pipes, such that a thermally driven, pulsating flow (and circulation) can transfer heat very efficiently from one part of the PHP to another in both sensible and latent forms. Unlike some conventional heat pipes, the PHPs can also work in a vertical orientation, even with the evaporator section located at the top in normal gravity.

In addition to a typical model shown in Fig. 1, PHPs can have slightly different structures. Maezawa et al.[2] proposed three structures: 1) looped with check valves, 2) looped without check valves, and 3) unlooped without check valves. Lin et al.[3] reported experimental results for an unlooped structure with different working fluids. For electronics cooling, Zuo et al.[4] developed a high heat flux structure of a pulsating loop combined with a wick material. Miyazaki et al.[5] found that check valves can improve the operating limits of looped PHPs.

There has been an increasing amount of research[6–16] on the working mechanisms of this heat transport device in recent years. Although the two-phase flow characteristics occurring inside the PHPs is highly complex due to phase change and interactions between the liquid slugs and vapor bubbles, several models have been developed to describe the complex two-phase flow based on rough assumptions. However, it appears that none of the existing models have considered the effect of surface tension at the meniscus, which affects the driving force for the pulsating flow. Recently, Khandekar et al.[17] reported on a study of PHPs operating as a single-phase thermosyphon, trying to understand the underlying principles of PHP operation. Recently, Khandekar et al,[11] Charoensawan et al.,[12] and Khandekar et al.[13] identified that gravity does play a role in the PHP action, and a series of inclination angles were tested against the PHP operations. To date, there are still no reliable data or tools available to achieve optimum PHP designs.[16,17]

In this work, the effect of gravity on the performance of PHPs was studied theoretically and experimentally to determine whether PHPs can be developed for space applications. Reduced-gravity experiments were performed to obtain data aboard Falcon-20 aircraft flying parabolic trajectories. The parabolic flight experiments have clearly shown improved heat transfer performance under reduced gravity.

Theoretical Considerations

Vapor Plug Formation

In a PHP, the working fluid undergoes phase change and forms liquid slugs and vapor plugs, which travel between the evaporator and condenser sections and sustain a pulsating movement. From an analysis of gravity and surface tension forces acting on a vapor bubble in a channel, Hosoda et al.[18] derived an expression for the maximum channel diameter that can hold a stable vapor plug:

$$D_{\max} = 1.84\sqrt{\sigma/g(\rho_l - \rho_v)} \tag{1}$$

With this equation, the maximum channel diameter for normal gravity operation ($1\ g_0 = 9.81\ \text{m/s}^2$) is calculated to be $D_{\max} = 2.5$ mm for water and 1.5 mm for R-114 at 300 K. The currently available PHPs typically have channel diameters of $1 \sim 2$ mm that are consistent with these predictions. Under microgravity conditions (where $g \approx 0$), however, Eq. (1) predicts unrealistically large maximum channel diameters (for example, $D_{\max} = 15$ mm at $0.01g_0$ and 150 mm at $10^{-4}g_0$ for R-114) for sustaining a stable vapor plug. However, as the channel diameter is increased, the ratio of heat transfer area (inner surface area of the channel) to fluid volume decreases, which would most likely decrease the driving force for pulsating flow. Also, in a large diameter channel, the vapor–liquid interface can become unstable and break up, resulting in the generation of small bubbles and bubbly flow rather than slug flow. Thus, Eq. (1) may not be suitable for use in the determination of the maximum channel diameter for PHPs used in microgravity. The maximum channel diameter for PHP operation in microgravity is examined further hereafter.

Flow Patterns Under Microgravity

It is clear that to maintain a strong pulsating flow in a PHP, the two-phase flow pattern in the channel needs to be kept in a slug/plug flow pattern. With a lack of buoyancy in the microgravity environment, gas–liquid flows, in general, have simpler flow patterns than those on the ground. Only three distinct two-phase flow patterns have been reported typically to exist in a μg environment, that is, bubbly, slug, and annular flows. Jayawardena et al.[19] developed a pair of flow pattern transition maps using dimensionless numbers and suggested the importance of a Suratman number in determining the transition boundaries between the flow patterns:

$$Su = \rho_l \sigma D \big/ \mu_l^2 = Re_l^2 \big/ We_l \tag{2}$$

This dimensionless number describes the competition among inertia, viscous, and surface tension forces. It has been found that when the Suratman number is used to describe slug–annular flow pattern transition, the proposed transition boundary depends greatly on the range of Suratman number. This implies that there are probably additional or other factors that could better describe the transition than the Suratman number alone.

Lin et al.[3] noted that the velocity is an important factor for flow pattern transition and used the following dimensionless superficial vapor velocity to formulate flow pattern transition criteria:

$$j_g^* = \frac{V\rho_v^{0.5}}{[gd_i(\rho_l - \rho_v)]^{0.5}} \tag{3}$$

This dimensionless velocity includes gravitational acceleration and describes the competition between inertia and gravity forces. For microgravity, this parameter would have a large value for any superficial vapor velocity; thus, it would not be suitable for the prediction of the flow pattern transition.

Channel Diameter and Flow Patterns in a PHP Under Microgravity

Under microgravity conditions, there is no gravity force to separate the liquid and vapor phases, and slug/plug flow patterns form more easily compared with the situation under gravity. The following analysis is intended to identify the factors that control the flow patterns under microgravity.

In the capillary tube of a PHP, vapor and liquid slugs travel as shown in Fig. 2, where the tail and nose of a vapor plug are indicated in front of and behind a liquid slug, respectively.[10] The factors controlling the pulsating slug flow in PHPs are considered to be the impulsive (inertia) force due to vapor nucleation and rapid expansion in volume, and the surface tension force. A similar idea was used by Zhao and Hu[20] to build a model for slug to annular flow transition under microgravity, although they considered the impulsive force of gas. In PHPs, the liquid and vapor slugs appear to move together with almost the same velocity (from the visualization experiment of Ref. 21), so that the liquid inertia is considered to be more dominant because of its higher density. Surface tension is also important to maintain the vapor/liquid interface shape and

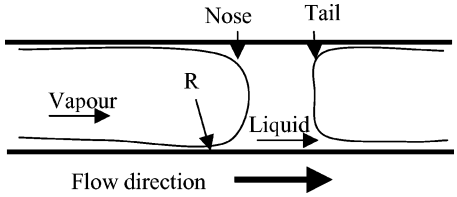

Fig. 2 Stability of a liquid slug.

to prevent the liquid slugs from disintegrating and the flow pattern from changing to churn or annular flow.

The kinetic energy of the liquid slug can be described by

$$E_k = \tfrac{1}{2}\rho_l V^2 \tag{4}$$

The surface energy can be approximately calculated if we take the tube radius as the radius of curvature for the meniscus:

$$E_s = \sigma / r \tag{5}$$

We assume that, when $E_s \geq k \cdot E_k$, a stable slug/plug flow pattern is maintained, where k is a constant of the order one in magnitude. A simple stability criterion can then be derived from Eqs. (4) and (5),

$$\sigma / r \geq k \tfrac{1}{2}\rho_l V^2 \tag{6}$$

so that

$$r \leq 2\sigma \big/ k\rho_l V^2 \tag{7}$$

From Eq. (7), it can be concluded that, for a typical PHP to sustain a pulsating flow under microgravity, the diameter of the channel is still very critical. The channel diameter must be sufficiently small to maintain a plug/slug flow pattern in the PHPs under microgravity.

By rearranging Eq. (6), we can estimate the value of k from

$$1/k = \tfrac{1}{2}\left(\rho_l V^2 r \big/ \sigma\right) = \tfrac{1}{4}\left(\rho_l V^2 D \big/ \sigma\right) = \tfrac{1}{4} \cdot We \tag{8}$$

where

$$We = \rho_l V^2 D \big/ \sigma \tag{9}$$

is the Weber number often used to account for surface tension in two-phase flow.[22,23]

Zhao and Hu[20] used $k = 0.8$ for their semi-empirical model of slug-to-annular flow transition in microgravity. In this work, we assume that $k = 1$ and that the mean velocity V is 0.12 m/s for the fluid used in this work, R-114, based on a visualization study.[21] Then, from Eq. (7), we obtain $r = 2.5$ mm, so that the critical channel diameter would be 5 mm for PHPs filled with R-114 under microgravity. This diameter is significantly greater than 1.5 mm for ground operation from Eq. (1), which suggests that the PHPs could use much larger channel diameters for space applications.

If the channel diameter is larger, the flow resistance will be lower, and the slug velocities will be higher. As a result, a smaller driving force due to phase change would suffice to sustain oscillating slug flows in the PHP. However, under normal gravity, surface tension may not be able to overcome the gravitational force in larger channels, as Eq. (1) suggests. For example, in large horizontal channels, phase separation can occur and slug/plug flows may change into stratified flow. In large vertical channels, bubbly and churn flow patterns can occur that will adversely affect the pulsating motion and heat transfer performance of the PHPs. Because these problems will be absent under microgravity, increasing the channel diameter would not be problematic for PHP operation under microgravity.

For the same channel diameter, the PHPs are also expected to work more efficiently in microgravity than under normal gravity for nonhorizontal orientations. When the PHP is placed vertically under normal gravity and the condenser section is located at the bottom, the driving force for liquid slugs to move upward will be opposed by gravity. This problem will be eliminated if the evaporator section is placed at the bottom under normal gravity. Thus, in a microgravity environment the PHPs with small or large channels are expected to perform better regardless of the heat pipe orientation.

Experimental Apparatus

PHP Models

Two PHP models used in the parabolic flight experiments are shown in Figs. 3 and 4. They were of the same outer size, $250 \times 60 \times 2.2$ mm, made of a thin aluminium plate and charged with R-114 as a working fluid at a fill ratio of $50 \sim 60\%$. The inner

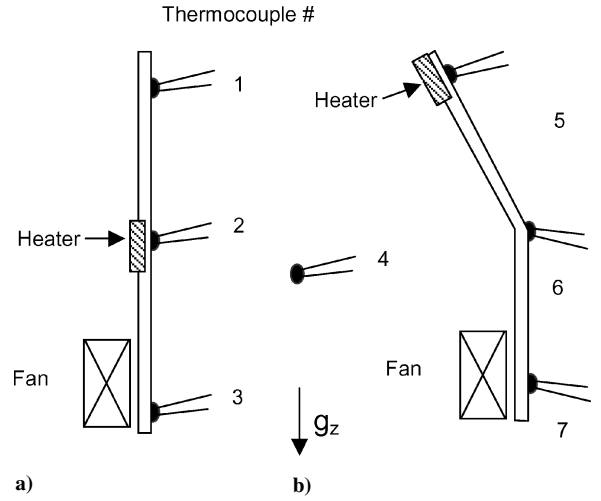

Fig. 3 PHP models and orientation in parabolic flights 1 and 2: a) heat pipe 1 and b) heat pipe 2.

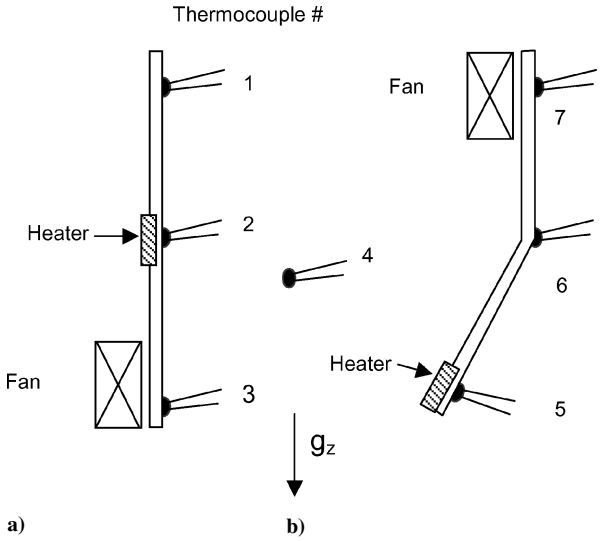

Fig. 4 PHP models and orientation in parabolic flights 3 and 4: a) heat pipe 1 and b) heat pipe 2.

channel consisted of a single continuous channel with a 1×1 mm cross section, laid out in a serpentine pattern with 48 turns at both ends.

The locations of K-type thermocouples (Omega), an electric heater, and a fan attached to each heat pipe are also indicated in Figs. 3 and 4. The heater used for both heat pipes was a Kapton® heater (55×16 mm) cemented onto the outer surface of the PHP and connected to a dc power supply providing $1.4 \sim 5.9$ W. The model 1 heat pipe was flat in shape and had the heater attached in the middle and a fan at one end, whereas the bent heat pipe model 2 had the heater and fan positioned at opposite ends. The fans were 80×80 mm in size with blade diameters of 75 mm (model 1) and 70 mm (model 2), respectively, and mounted 70 mm away from the heat pipe surface to reject heat. The center of the fan was positioned 60 mm from one end of each heat pipe. The model 1 used a dc fan rated at 3.5 W and 0.91 m^3/min (flow rate), whereas the model 2 fan was rated at 3.5 W and 1.25 m^3/min (flow rate). The average air velocity at the face of the fan is calculated to be 3.4 m/s (model 1) and 5.4 m/s (model 2), respectively.

In the model 1 experiments, forced air cooling was provided by the fan at one end and by natural convection at the other end under normal gravity. Under reduced gravity, the airflow due to natural convection was suppressed, and so cooling must have occurred only at the opposite end. In the model 2 experiments, two different orientations were tested: 1) heater located at the top and cooling fan at

the bottom and 2) heater at the bottom and cooling fan at the top. In both PHP models, the directions of internal fluid flow and heat transport were parallel.

Experimental Uncertainty

The uncertainty in the temperature data collected by the data acquisition system was estimated to be $\pm 0.2^{\circ}$C. The uncertainty in the acceleration data was within $\pm 0.001 g_0$.

Microgravity Environment

The aircraft flew a parabolic trajectory and provided alternating periods of normal-, hyper-, and reduced-gravity conditions.[24] Each parabola consisted of three different phases:

Phase 1, where, starting from a horizontal trajectory ($\sim 1 g_0$) at an altitude of 20,000–26,000 ft (6000–8000 m), the aircraft accelerated upward at an angle of approximately 45 deg from horizontal. In this entry pullup maneuver, the vertical acceleration level g_z increased to about 1.8–2.5 g_0, and the aircraft kept climbing for ~15 s, until it reached an altitude of ~26,000 ft (8000 m).

Phase 2, where the engine power was considerably reduced during the next 15–20 s, so that the aircraft was in a free-fall condition. This was the reduced gravity period, in which an object in the aircraft cabin behaved as if it had no weight for a period of 15–20 s. After reaching a peak altitude of ~26,000 ft (~8000 m), the aircraft entered a downward trajectory.

Phase 3, where, when the aircraft's angle reached a −45-deg trajectory from horizontal, the engine power was restored and the aircraft started to accelerate upward (called exit pull up) for about 20 s to enter a horizontal trajectory and a normal-gravity condition, completing one parabola.

Each parabolic flight provided four reduced gravity periods of 15–20 s duration. Figure 5 shows typical variations of acceleration levels recorded during the second parabolic flight flown in this work: A_x, longitudinal direction pointing to the fore of the aircraft; A_y, spanwise direction toward the right wing of the aircraft; and A_z, upward vertical direction. The acceleration levels were measured by a three-axis accelerometer installed on the aircraft, and the data were recorded at a sampling frequency of 32 Hz. The accelerometer signal was also connected to the data acquisition system belonging to the experimental apparatus, so that the temperature and acceleration data could be synchronized for later analysis.

As is evident from Fig. 5 and the acceleration data for other flights, the vertical acceleration level A_z varied between ~0 and ~2.5 g_0 in accordance with the parabolic trajectory just described, whereas the acceleration levels in the fore–aft direction A_x, and spanwise direction A_y, changed only slightly during the entire flight.

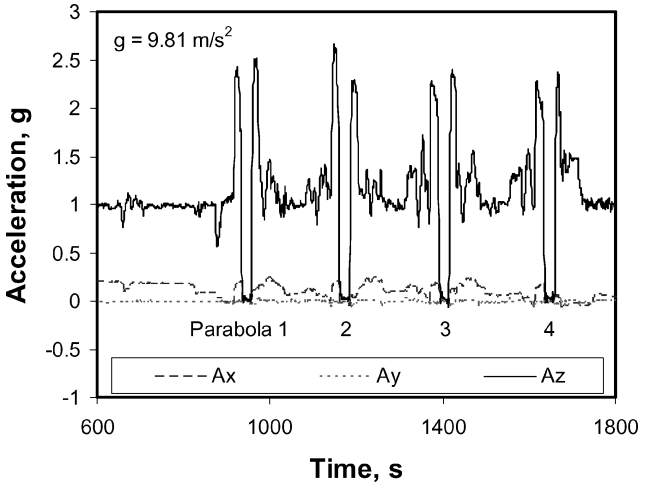

Fig. 5 Variation of acceleration levels in three directions during flight 2.

Experimental Results and Discussion

Temperature and Pressure Profiles During the Flights

Figures 6–13 show the temperature profiles of the two aluminium PHP models tested and the acceleration level A_z during the parabolic flight experiments. The acceleration profiles shown in Figs. 6–13 indicate the reduced-gravity periods when the vertical acceleration level falls to near zero. Although the pressure variation in the aluminium PHPs was not measured, the pressure data from another tubular PHP instrumented with a pressure transducer and based on the same principle of operation suggested relatively constant pressure in the aluminium PHPs during the parabolic flights.

Midsection Heated Model 1

Model 1 was heated in the middle, as shown in Fig. 3. Figures 6–8 show the temperature data for heater power inputs of 1.1, 2.5, 4.4 and 5.9 W. In Figs. 6–8, T_1 is the temperature at the top of the heat pipe where there was no fan and only natural convective cooling by ambient air existed during normal and hypergravity. Natural convection was suppressed under reduced gravity. T_2 is the temperature in the midsection where the Kapton heater was attached. T_3 is the temperature at the bottom of the heat pipe where it was cooled by an electric fan.

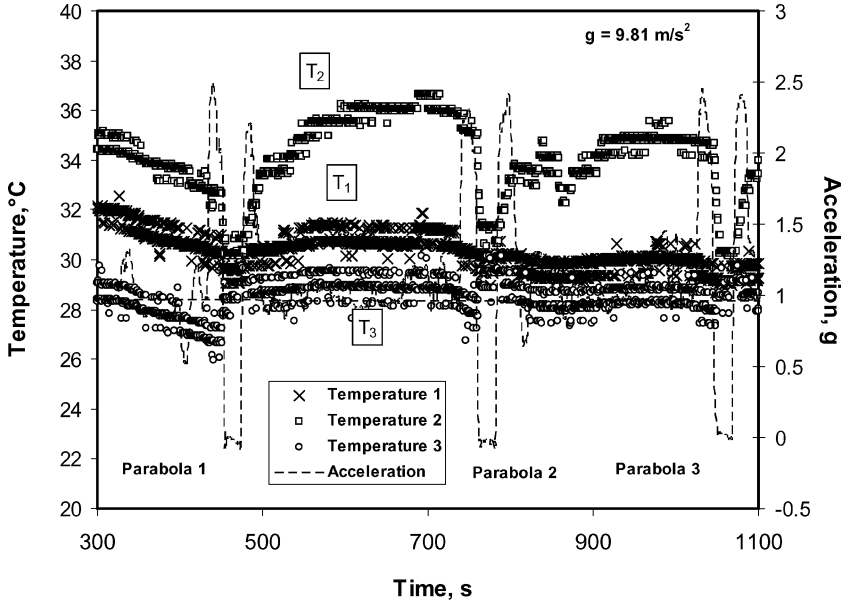

Fig. 6 Temperature profiles of model 1 (midheating) during flight 1, heating power = 4.4 W.

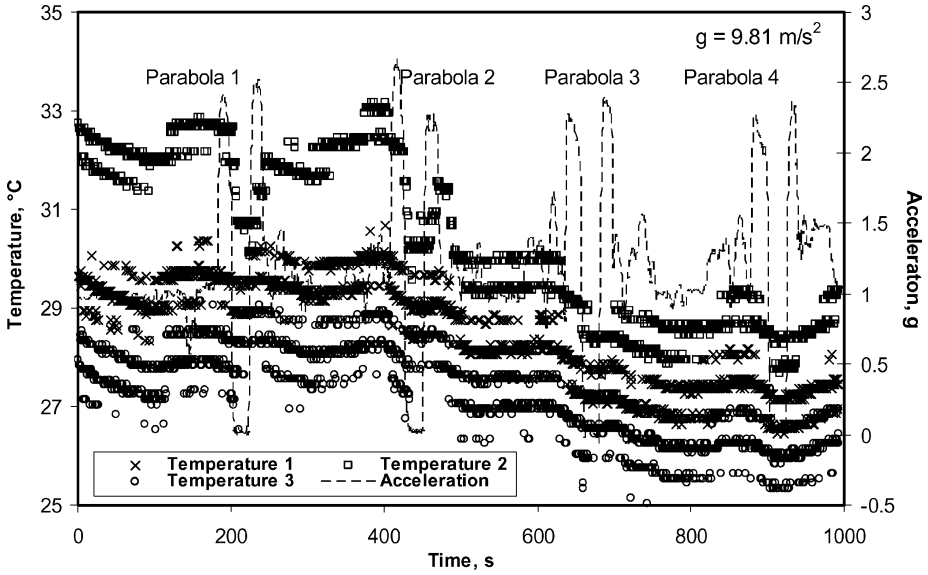

Fig. 7 Temperature profiles of model 1 (midheating) during flight 2, with a heater power of 2.5 W for parabolas 1–2 and 1.1 W for parabolas 3–4.

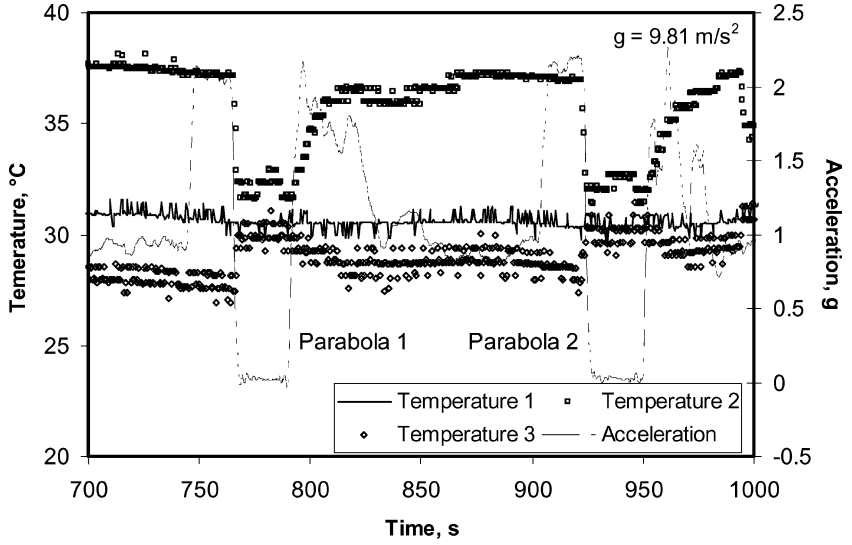

Fig. 8 Temperature profiles of model 1 (midheating) during flight 4, heater power of 5.9 W.

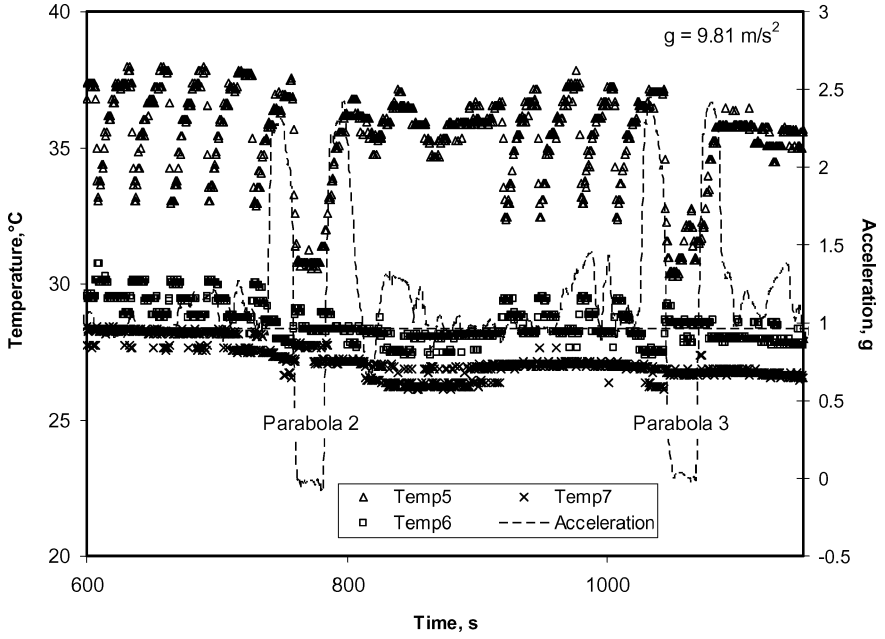

Fig. 9 Temperature profiles of model 2 (top heating) during flight 1, heater power is 4.4 W.

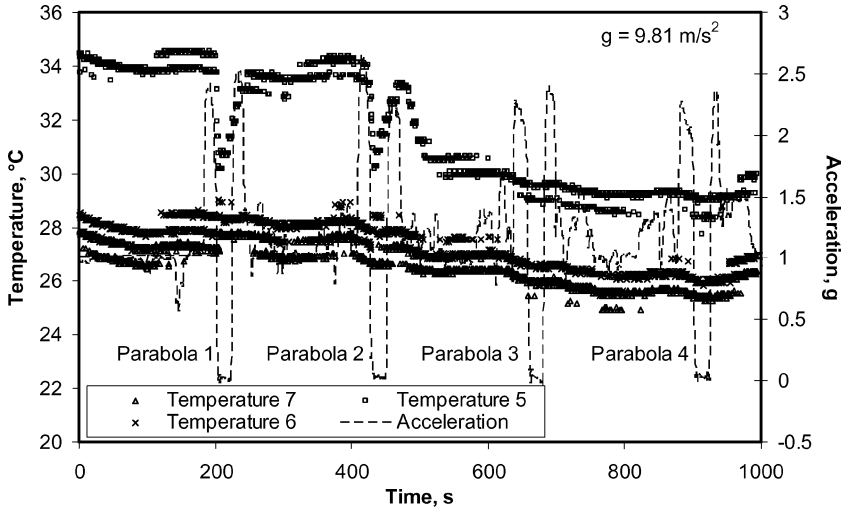

Fig. 10 Temperature profiles of model 2 (top heating) during flight 2, heater power is 2.5 W for parabolas 1–2 and 1.1 W for parabolas 3–4.

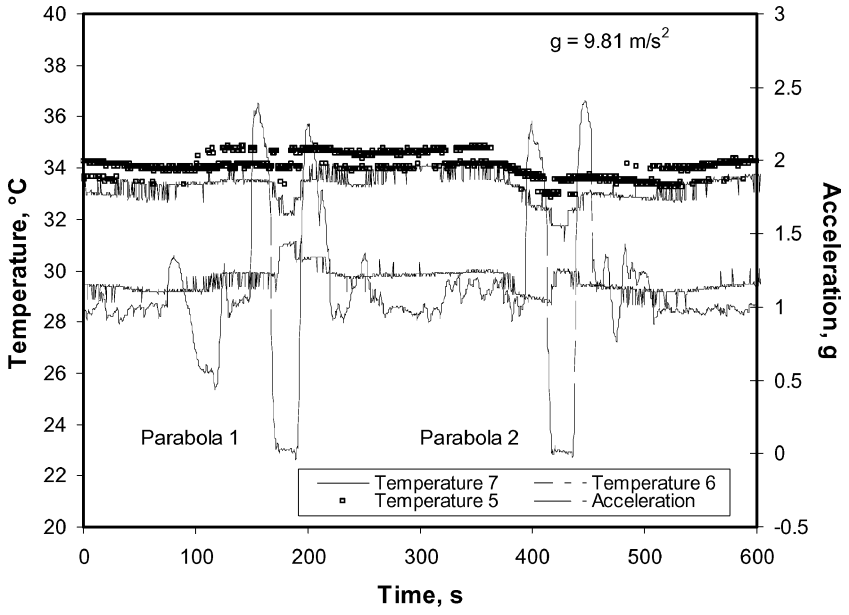

Fig. 11 Temperature profiles of model 2 (bottom heating) during flight 3, heater power is 4.4 W.

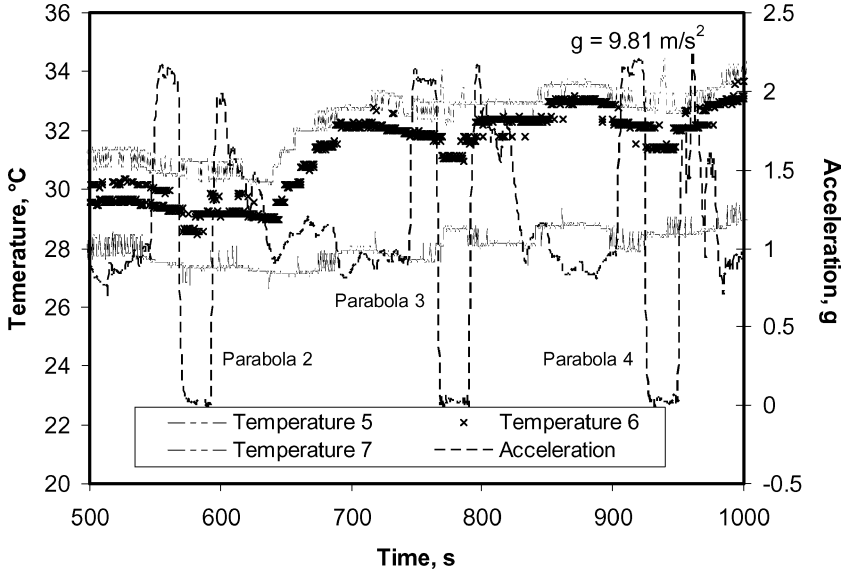

Fig. 12 Temperature profiles of model 2 during flight 4 with different heater power applied at the bottom: 2.5 W for parabolas 2 (the first from left), and 5.9 W for parabolas 3 and 4.

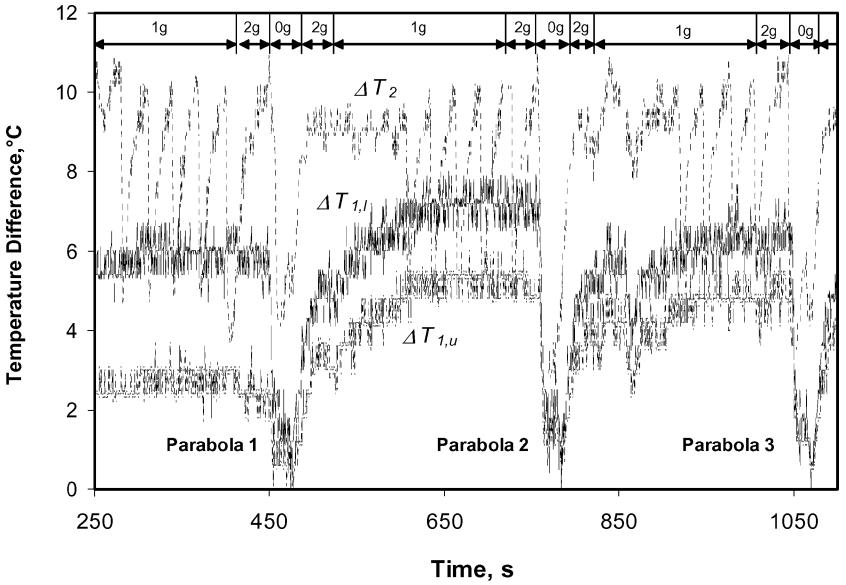

Fig. 13 Temperature differences during flight 1, heater power is 4.4 W.

In all cases, the temperature at the heated section T_2 was the highest, and the fan-cooled section T_3 the lowest. The top section, which was cooled by natural convection under normal/hypergravity showed an intermediate temperature between T_2 and T_3. The temperature profile data showed that the temperature difference between the heated and cooled sections became significantly reduced as the gravity level decreased from normal/hypergravity to reduced-gravity levels. The reduction in this temperature difference was more significant at higher levels of heater power input.

Model 2 Data: Heating at the Top or Bottom

Model 2 was heated at the top in the first two flights, and at the bottom in flights 3 and 4, as shown in Figs. 3 and 4. In both cases, T_5 is the temperature at the heated section, T_6 is the temperature in the middle of the heat pipe, and T_7 is the temperature at the cooled section, where a cooling fan was used to provide forced air cooling.

The temperature data for the top heating case at heater power inputs of 1.1, 2.5, and 4.4 W are shown in Figs. 9 and 10, whereas the data for the bottom heating case are shown in Figs. 11 and 12 for heating power inputs of 2.5, 4.4, and 5.9 W. Unlike conventional heat pipes, the present PHP was able to function in the top heating mode under all gravity levels, as indicated by steady temperature profiles in Figs. 9 and 10. At a heater power input of 4.4 W, however, the heated section temperature T_5 showed large fluctuations with a period of ~ 30 s, possibly indicating partial dryout and rewetting due to an instability in the pulsating flow inside the PHP. At other heater power levels, the heat transport performance in the top heating case was not as good as that for the midheating case, as indicated by the larger temperature differences between the heated and cooled sections at the same heater power level.

The bottom heating case yielded smaller temperature differences at normal and hypergravity levels, indicating better heat transport in the heat pipe, in comparison with the data from the midheated model 1. As the gravity level changed from $\sim 2g_0$ to near zero, the temperature difference between the heated and cooled sections again decreased, and this reduction was greater at higher heater power levels, as was seen for the model 1 results.

In the next section, the thermal performance is evaluated and compared among the different cases.

Heat Transport Analysis

To analyze the heat transfer performance of the two PHP models tested quantitatively, the temperature differences were first calculated as follows:

$$\Delta T_{1,u} = (T_2 - T_1)/2 \tag{10}$$

$$\Delta T_{1,l} = (T_2 - T_3)/2 \tag{11}$$

$$\Delta T_2 = (T_5 - T_7) \tag{12}$$

For model 1, $\Delta T_{1,u}$ is evaluated between the heated and natural convection cooled sections, or the upper-half of the heat pipe, whereas $\Delta T_{1,l}$ is the temperature difference between the heated and forced convection cooled sections. For model 2, ΔT_2 is the temperature difference between the heated and cooled sections located at the opposite ends.

Figure 13 shows the temperature differences obtained during flight 1 for both models. The fluctuation of temperature difference for model 2 in the top-heating case was violent under a $1g$ condition and deceased significantly when the heat pipe entered the reduced gravity period. For model 1, similar reductions in the temperature difference could be observed. It is clear that at a reduced-gravity level, the temperature difference is minimized, and a more uniform temperature distribution over the entire heat pipe length can be obtained.

The thermal resistances ($\Delta T/q$) of both heat pipe models were then calculated based on the temperature differences shown in Fig. 13. For model 1, the average temperature difference between $\Delta T_{1,u}$ and $\Delta T_{1,l}$ was used. As shown in Fig. 14, the thermal resistance ranged between about 1 and 2.4 K/W for both models under normal and hypergravity. The thermal resistance of the top-heated model fluctuated between 2.3 and 1.1 K/W under normal and hypergravity, possibly due to the partial dryout and rewetting phenomena in the evaporator section. However the lowest value of $\sim$1 K/W reached was the same as that of the midsection heated model 2.

Under reduced gravity, the thermal resistances fell significantly in both models. For the midsection heated model 1, the thermal resistance of $\sim$0.3 K/W reached was about one-third of its normal gravity value. This indicates that gravity hinders rather than helps the fluid movement and heat transport characteristics of a PHP.

Effects of Heating Loads, Gravity, and Orientation

The thermal resistance decreased with the heater power for both normal and reduced gravity operations as shown in Fig. 15, where the thermal resistances averaged over the normal-gravity and reduced-gravity periods are shown against the heater power. At a low heater power, $q \sim 1$ W, the pulsating flow was weak both under normal and reduced gravity, and relatively high thermal resistances were obtained for all of the heater locations and heat pipe orientations. However, at a higher heater power, increasingly stronger pulsating flows led to better heat transport performance for the midsection heated and top heated PHPs. For the bottom heated model 2, the

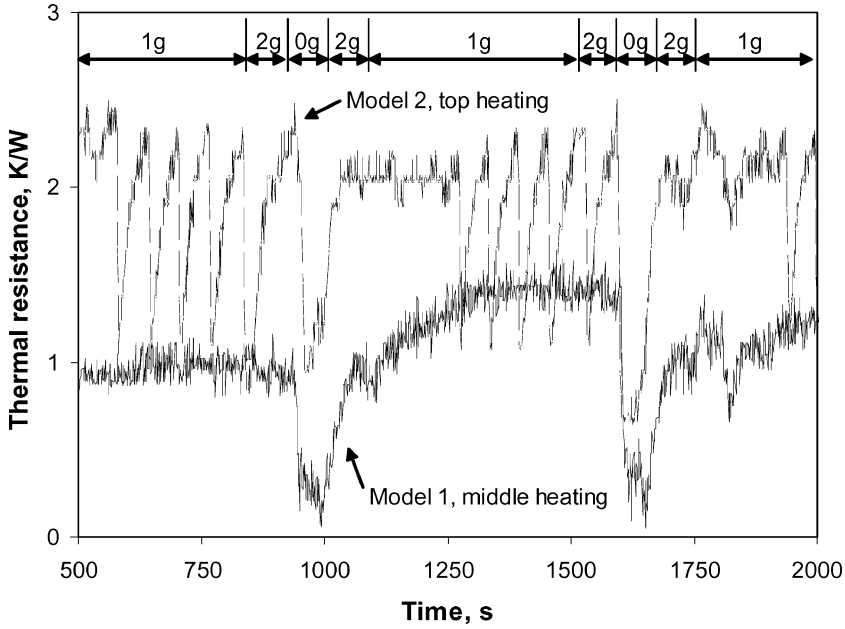

Fig. 14 Variation of thermal resistance with gravity level, heater power is 4.4 W.

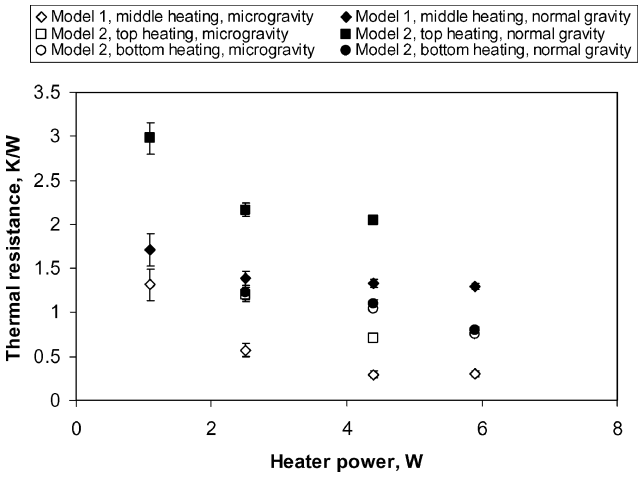

Fig. 15 Improvements in PHP performance with heater power under reduced gravity.

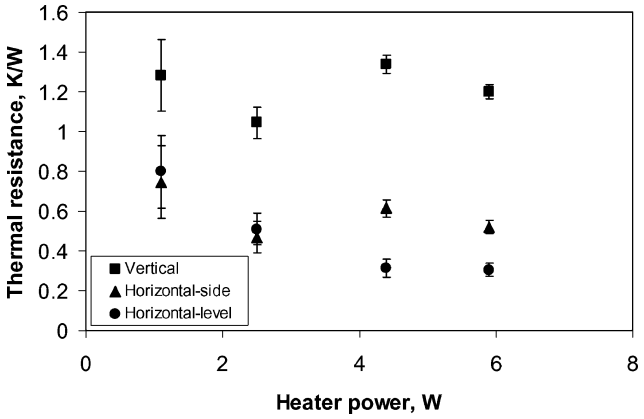

Fig. 16 Orientation effects on the heat transport performance of midsection heated PHP (model 1) under normal gravity.

improvements were small because its pulsating flow was probably sufficiently strong even under normal gravity.

Under normal gravity, the bottom heating case gave the best performance, followed by the midheating, and then the top heating cases. When heated at the top, the heat transfer performance of model 2 was relatively poor and unsteady under $1\,g_0$, but significantly improved during the reduced gravity periods.

Figure 16 shows the thermal resistances of midsection heated model 1 operating on the ground ($1\,g_0$) in different orientations: vertical, horizontal-side, that is, horizontal but lying on its side, and horizontal-level (horizontal and flat). The horizontal-level orientation was very close to the microgravity environment because the direction of the pulsating flow was perpendicular to gravity, and no hydrostatic effects would be present. Indeed, the thermal resistance obtained for the horizontal-level orientation, $\Delta T/q = \sim 0.3$ K/W at >4 W power input, was close to the average $\Delta T/q$ values obtained during reduced gravity periods for the midsection heated case, as shown in Fig. 15.

The effects of gravity on the operation of the current PHPs tested in vertical and horizontal orientations shown in Figs. 15 and 16 support the hypothesis that the PHPs with larger channel diameters can operate under microgravity as suggested by Eq. (7). Because the PHP operation is unaffected by gravity in the horizontal-level orientation, the pulsating vapor–liquid two-phase flow and heat transport mechanisms under microgravity are not expected to significantly change in the enlarged heat pipe channels, due, for example, to the phase separation phenomena.

Conclusions

The operation of PHPs under reduced gravity was investigated experimentally via parabolic flight experiments aboard Falcon 20 aircraft. Two thin aluminium PHPs charged with R-114 were instrumented with thermocouples to measure the temperature variations at the evaporator and condenser sections during which gravity level changed between hypergravity ($\sim 2\,g_0$) and reduced gravity ($\sim 0.02\,g_0$).

During the parabolic flight experiments, both heat pipe models showed better operating characteristics and improved heat transfer performance under reduced gravity than under normal or hypergravity. The experimental results strongly suggest that the PHPs can operate satisfactorily under long-term microgravity and, thus, they can be reliably deployed for space applications. Under normal and hypergravity, the orientation of the PHPs and positions of evaporator/condenser sections relative to gravity were found to be important for their operation and heat transport performance. Placement a heater (evaporator section) at a lower position would prevent

unstable operation and temperature fluctuations because gravity helps the liquid to flow back to the evaporator section and helps the vapor to rise to the condenser section more easily.

The performance of the PHPs tested was further examined by evaluation of the thermal resistance from the heat load and temperature difference between the heated and cooled sections. Under normal gravity, the thermal resistance ranged from about 0.8 to 3 K/W, but decreased to about $0.3 \sim 0.8$ K/W under reduced gravity for all orientations. The performance of the PHP in horizontal orientation was not affected by gravity as expected, and the thermal resistance was as low as 0.3 K/W, even under normal gravity at heater power levels of 4.4 and 5.9 W.

Theoretical considerations revealed the possibility that PHPs with larger channel diameters (up to 5 mm for R-114 as a working fluid) may be able to operate satisfactorily under microgravity, though they may not work on the ground. The predicted maximum diameter is significantly greater than the limiting value for the ground operation calculated from Eq. (1) (1.5 mm for R-114), thus, it can be hypothesized that the PHPs could use larger channel diameters for space applications and transport more heat in the absence of gravity. The effect of gravity observed on the operation of the current PHPs tested in vertical and horizontal orientations under normal gravity, and the results of the parabolic flight experiments, lend support to this hypothesis.

Acknowledgments

This work was financially supported by the National Space Development Agency of Japan, and the parabolic flight opportunity was provided by the Canadian Space Agency (CSA) aboard Falcon 20 aircraft operated by the National Research Council (NRC) of Canada. The authors thank Eric Vachon of CSA and the staff at NRC for their help in conducting the parabolic flight experiments.

References

[1]Akachi, H., and Polasek, F., "Pulsating Heat Pipes, Heat Pipe Technology: Theory, Applications and Prospects," *Proceedings of the 5th International Heat Pipe Symposium*, Pergamon, Oxford, England, U.K., 1996, pp. 208–217.

[2]Maezawa, S., Nakajima, R., Gi, K., and Akachi, H., "Experimental Study on Chaotic Behavior of Thermohydraulic Oscillation in Oscillating Thermosyphon," *Proceedings of the 5th International Heat Pipe Symposium*, Pergamon, Oxford, England, U.K., 1996.

[3]Lin, L., Ponnapan, R., and Leland, J., "Experimental Investigation of Oscillating Heat Pipes," *Journal of Thermophysics and Heat Transfer*, Vol. 15, No. 4, 2001, pp. 395–400.

[4]Zuo, Z. J., North, M. T., and Ray, L., "Combined Pulsating and Capillary Heat Pipe Mechanism for Cooling of High Heat Flux Electronics," *Proceedings of the ASME Heat Transfer Division*, HTD-Vol. 364-4, American Society of Mechanical Engineers, Fairfield, CT, 2000, pp. 237–243.

[5]Miyazaki, Y., Akachi, H., and Polasek, F., "Oscillating Heat Pipe with Check Values," *6th International Heat Pipe Symposium* [CD-ROM], National Science and Technology Development Agency of Thailand and Japan Association of Heat Pipes, Tokyo.

[6]Ma, H. B., Hanlon, M. A., and Chen, C. L., "An Investigation of Oscillation Motions in a Pulsating Heat Pipe," *Proceedings of the 35th National Heat Transfer Conference* [CD-ROM], American Society of Mechanical Engineers, New York, 2001.

[7]Zhang, Y., and Faghri, A., "Heat Transfer in a Pulsating Heat Pipe with Open End," *International Journal of Heat and Mass Transfer*, Vol. 45, No. 4, 2002, pp. 755–764.

[8]Shafii, M. B., Faghri, A., and Zhang, Y., "Thermal Modeling of Unlooped and Looped Pulsating Heat Pipes," *Journal of Heat Transfer*, Vol. 123, No. 6, 2001, pp. 1159–1172.

[9]Wong, T. N., Tong, B. Y., Lim, S. M., and Ooi, K. T., Theoretical Modelling of Pulsating Heat Pipe," *Proceedings of the 11th International Heat Pipe Conference*, Japan Association for Heat Pipes, Tokyo, Japan, 1999.

[10]Tong, B. Y., Wong, T. N., and Ooi, K. T., "Closed-Loop Pulsating Heat Pipe," *Applied Thermal Engineering*, Vol. 21, No. 18, 2001, pp. 1845–1862.

[11]Khandekar, S., Dollinger, N., and Groll, M., "Understanding Operational Regimes of Closed Loop Pulsating Heat Pipes: An Experimental Study," *Applied Thermal Engineering*, Vol. 23, No. 6, 2003, pp. 707–719.

[12]Charoensawan, P., Khandekar, S., Groll, M., and Terdtoon, P., "Closed Loop Pulsating Heat Pipes—Part A: Parametric Experimental Investigations," *Applied Thermal Engineering*, Vol. 23, No. 16, 2003, pp. 2009–2020.

[13]Khandekar, S., Charoensawan, P., Groll, M., and Terdtoon, P., "Closed Loop Pulsating Heat Pipes—Part B: Visualization and Semi-Empirical Modeling," *Applied Thermal Engineering*, Vol. 23, 2003, pp. 2021–2033.

[14]Shafii, M. B., Faghri, A., and Zhang, Y., "Analysis of Heat Transfer in Unlooped and Looped Pulsating Heat Pipes," *International Journal of Numerical Methods for Heat and Fluid Flow*, Vol. 12, No. 5, 2002, pp. 585–609.

[15]Zhang, Y., and Faghri, A., "Oscillatory Flow in Pulsating Heat Pipes with Arbitrary Numbers of Turns," *Journal of Thermophysics and Heat Transfer*, Vol. 17, No. 3, 2003, pp. 340–347.

[16]Schneider, M., Khandekar, S., Kulenovic, R., Schäfer, P., and Groll, M., "Visulization of Thermodynamic Phenomena in Flat Plate Closed Loop Pulsating Heat Pipes," *6th International Heat Pipe Symposium* [CD-ROM], National Science and Technology Development Agency of Thailand and Japan Association of Heat Pipes, Tokyo.

[17]Khandekar, S., Groll, M., Charoensawan, P., and Terdtoon, P., "Pulsating Heat Pipes: Thermo-Fluidic Characteristics and Comparative Study with Single Phase Thermosyphon," *12th International Heat Transfer Conference*, Vol. 4, Elsevier, New York, 2002, p. 459.

[18]Hosoda, M., Nishio, S., and Shirakashi, R., "Meandering Closed-Loop Heat Transport Tube (Propagation Phenomena of Vapor Plug)," *Proceedings of the 5th ASME/JSME Joint Thermal Engineering Conference*, American Society of Mechanical Engineers, New York, 1999.

[19]Jayawardena, S. S., Balakotaiah, V., and Witte, L. C., "Flow Pattern Transition Maps for Microgravity Two-Phase Flows Verified at Low Suratman Number Systems," *AIChE Journal*, Vol. 43, No. 6, 1997, pp. 1637–1640.

[20]Zhao, J. F., and Hu, W. R., "Slug to Annular Flow Transition of Microgravity Two-Phase Flow," *International Journal of Multiphase Flow*, Vol. 26, No. 8, 2000, pp. 1295–1304.

[21]Gu, J., and Kawaji, M., "Microgravity Performance of Pulsating Heat Pipes," *2nd International Symposium on Physical Sciences in Space* [CD-ROM], National Science and Technology Development Agency of Thailand and Japan Association of Heat Pipes, Tokyo.

[22]Rezkallah, K. S., "Weber Number Based Flow-Pattern Maps for Liquid–Gas Flows at Microgravity," *International Journal of Multiphase Flow*, Vol. 22, No. 6, 1996, pp. 1265–1270.

[23]Whalley, P. B., *Boiling, Condensation, and Gas-Liquid Flow*, Oxford Univ. Press, New York, 1987.

[24]"Falcon 20 User's Guide," Canadian Space Agency, St-Hubert, Quebec, Canada, May 2001.